Lyotropic Liquid Crystallinity of Linear and Cyclic Amylose Derivatives: Amylose Tris(*n*-octadecylcarbamate) in Tetrahydrofuran and 2-Octanone

DongChan Kim,[†] Akiyuki Ryoki,[†,‡] Daigo Kabata,[†] Shinichi Kitamura,[§] and Ken Terao[*,†]*

[†]Department of Macromolecular Science, Graduate School of Science, Osaka University, 1-1 Machikaneyama-cho, Toyonaka, Osaka 560-0043, Japan
[‡]Department of Polymer Chemistry, Graduate School of Engineering, Kyoto University, Katsura, Kyoto 615-8510, Japan
[§]Center for Research and Development of Bioresources, Organization for Research Promotion, Osaka Prefecture University, 1-2, Gakuen-cho, Naka-ku, Sakai, 599-8570, Japan

* Corresponding author. Tel.: +81 6 6850 5459; fax: +81 6 6850 5461.
E-mail address: kterao@chem.sci.osaka-u.ac.jp

ABSTRACT: Lyotropic liquid crystallinity was examined for 8 linear amylose tris(*n*-octadecylcarbamate) (ATODC) samples ranging in the weight-average molar mass (M_w) from 25 kg mol^{-1} to 1510 kg mol^{-1} and 10 cyclic ATODC (cATODC) samples, M_w of which varies between 36 kg mol^{-1} and 191 kg mol^{-1}. Appreciable cholesteric patterns were not observed in the concentration range investigated. Diffraction data from small-angle X-ray scattering both for bulk polymer samples at 160 – 180 °C and concentrated solutions at 25 °C indicate that no characteristic peaks were found except for a broad diffraction reflecting the chain distance between the neighboring polymer molecules. The phase boundary concentrations for ATODC and cATODC in tetrahydrofuran (THF) and 2-octanone (MHK) were determined at 25 °C as a function of M_w. The obtained phase diagram for ATODC was well fitted by a conventional scaled particle theory (SPT) for the wormlike spherocylinder as in the case of the other stiff polymer systems. On the other hand, when we assumed that cATODC chains form rodlike structure in the nematic phase, the experimental data were successfully explained by a modified SPT, suggesting conformation of cATODC in the nematic phase is different from that in dilute solution.

Key Words: Stiff chain, ring polymer, nanoring, liquid crystallinity, phase diagram, scaled particle theory, small-angle X-ray scattering

Introduction

Anisotropic molecules, that is, not only rodlike but also other shaped molecules including disks and bending rods, may form various kinds of liquid crystal phases.[1] Lyotropic liquid crystallinity can be observed for rigid rodlike polymers including polypeptides, polyisocyanates, polysaccharides, and their derivatives.[2, 3] Previous studies for lyotropic liquid crystallinity of polymeric materials were however mostly limited to linear chains due to the difficulty to prepare rigid nonlinear polymers except for supercoiled cyclic DNA[4] and three-arm star polymers.[5, 6]

Taking into consideration that recent simulation work predicted specific smectic phase for rigid nanorings,[7-9] investigation for lyotropic liquid crystallinity of rigid ring polymers is so inviting.

We recently found that highly concentrated tetrahydrofuran (THF) solutions of cyclic amylose tris(*n*-butylcarbamate) (cATBC) showed appreciable birefringence[10] while cATBC behaves as rigid ring polymer with considerably high chain stiffness in THF.[11] Lower phase boundary concentrations were however desirable to discuss thermodynamics of rigid ring polymer-solvent systems without experimental difficulties. According to the scaled particle theory (SPT) for the linear wormlike chain, phase boundary concentrations become lower with increasing chain thickness at fixed chain length and stiffness.[2] Indeed, phase boundary concentrations for amylose alkylcarbamates tend to lower with increasing alkyl side chains from ethyl to hexyl groups in THF.[12] This suggests that linear and cyclic amylose tris(*n*-octadecylcarbamate)s (ATODC and cATODC) for which chemical structures are shown in Chart 1 are suitable to investigate their lyotropic liquid crystallinity since both ATODC and cATODC behave as stiff chains in solution.[13] We thus determined their phase boundary concentrations in 2-octanone (MHK) and THF. Small-angle X-ray scattering (SAXS) measurement was also carried out for bulk and concentrated ATODC and cATODC solutions to determine the local alignment of polymer chains in the liquid crystalline phase since they may also have thermotropic liquid crystallinity as in the case of polysaccharide derivatives with alkyl side groups.[14-16]

Chart 1. Chemical Structures of (a) ATODC and (b) cATODC.

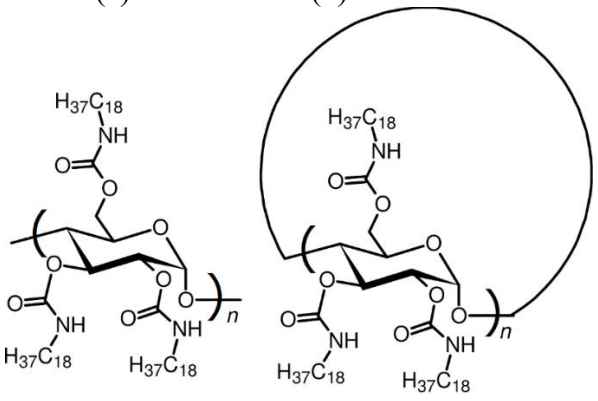

(a) ATODC (b) cATODC

Experimental Section

Samples. Previously investigated seven ATODC and four cATODC samples[13] prepared from enzymatically synthesized linear[17, 18] and cyclic[19, 20] amylose samples, respectively, were used for this study. The weight-average molar mass M_w and the dispersity index $Đ$ defined as the ratio of M_w to the number-average molar mass are summarized in Table 1. An ATODC and six cATODC samples were newly synthesized with the same procedure.[13] The chemical structure was confirmed by ^{1}H-NMR in chloroform-*d*, infrared absorption, and ultimate analysis. Size-exclusion chromatography equipped with multi-angle light scattering and refractive index detectors was performed for the newly prepared samples with THF as an eluent to determine M_w and $Đ$. These are also summarized in Table 1. The weight-average number of repeat unit can be calculated as M_w/M_0 with M_0 (= 1.049 kg mol^{-1}) being the molar mass per repeat unit. The resultant value ranges from 23 to 1400 for ATODC and from 34 to 190 for cATODC.

Table 1. Weight-average Molar Mass M_w and the Dispersity Index $Đ$ for ATODC and cATODC Samples

Sample	M_w (kg mol^{-1})	$Đ$
ATODC25K	24.6 [b]	1.08 [b]
ATODC38K	37.7 [b]	1.08 [b]
ATODC102K	102 [b]	1.10 [b]
ATODC155K	155 [a]	1.25 [a]
ATODC164K	164 [b]	1.18 [b]
ATODC284K	284 [b]	1.32 [b]
ATODC852K	852 [b]	1.51 [b]
ATODC1510K	1510 [b]	1.47 [b]
cATODC36K	36.1 [b]	1.16 [b]
cATODC45K	45.3 [a]	1.18 [a]
cATODC49K	49.0 [a]	1.15 [a]
cATODC58K	58.3 [a]	1.05 [a]
cATODC77K	77.1 [b]	1.15 [b]
cATODC89K	88.8 [a]	1.35 [a]
cATODC96K	95.9 [a]	1.09 [a]
cATODC122K	122 [b]	1.22 [b]
cATODC170K	170 [a]	1.13 [a]
cATODC191K	191 [b]	1.15 [b]

[a] From SEC-MALS. [b] Ref. 13.

Optical Microscopy and Small-Angle X-ray Scattering (SAXS). Thermal behavior was observed for **ATODC38K**, **ATODC155K**, and **cATODC77K** by using a melting point measuring instrument with Cross-Nicol optics with raising temperature. Weak birefringence was found around 150 °C and it disappeared around 180 °C. Similar behavior cannot be observed for amylose alkylcarbamates with shorter side chains in the temperature range investigated up to 210 °C since the phase transition temperature is much higher than that for ATODC. However, this phase transition behavior could not be observed by means of our DSC measurement. SAXS measurement was carried out for **ATODC38K**, **ATODC155K**, **ATODC852K**, **cATODC49K**, **cATODC77K**, and **cATODC170K** at the BL40B2 beamline in SPring-8. The camera length and the wavelength λ_0 of the incident X-ray were chosen to be 0.5 m and 0.077 nm, or 4 m and 0.1 nm, respectively, to cover a wide range of the magnitude q of the scattering vector. A PILATUS3S 2M silicon pixel detector (DECTRIS, Baden, Switzerland) was used to determine the scattering intensity I as a function of q since no significant azimuth angle dependence was observed. The same measurement was also performed for concentrated MHK solutions of some ATODC and cATODC samples.

Phase Separation Experiments of Concentrated Solution. Concentrated solutions both of ATODC and cATODC have two phase boundary concentrations, c_I and c_A. Here, c_I is the phase boundary concentration between isotropic and biphasic regions and c_A is that between biphasic and anisotropic regions. Phase separation experiments were therefore made for ATODC and cATODC samples in MHK and THF at 25 °C. Concentrated solutions for which initial concentration c_0 was adjusted to be between c_I and c_A were prepared in a conical vial with a screw cap in the following way. Cast film of each sample prepared from THF solution was weighed to put into the vial and an appropriate amount of solvent was added. The c_0 value was calculated from the weight ratio of the solute to the solution taking the solution density calculated with the partial specific volume $\bar{v}$ into consideration. The $\bar{v}$ value was determined to be 0.882 mL g^{-1} and 0.884 mL g^{-1} in MHK and THF, respectively, by using an Anton Paar DMA5000 densitometer. We utilized a vortex mixer to dissolve the sample. Furthermore, the mixture was centrifuged by using an angle rotor several times to knead and homogenize the solution around 30 °C; it should be noted that the MHK solutions were heated to 65 °C to attain complete dissolution. The resultant solution was further centrifuged with a swing rotor at 25 °C to attain two phase separation as shown in Figure 1. The meniscus height was determined by using a traveling microscope to determine the volume fraction Φ_{LC} of the liquid crystal phase at fixed c_0. The vial was calibrated with water to determine the relationship between volume and the meniscus height. While ATODC and cATODC are the chiral polymers, cholesteric color was not observed, indicating even though these systems have the cholesteric structure, the pitch is far from the wavelength of visible light.

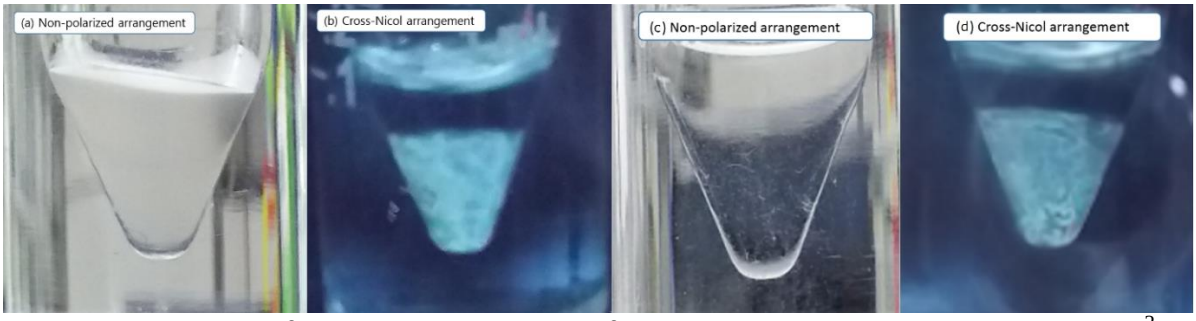

Figure 1. Photographs for coexistence phases of **ATODC155K** (a) (b) (c_0 = 0.24 g cm^{-3}) and **cATODC77K** (c) (d) (c_0 = 0.38 g cm^{-3}) in tetrahydrofuran (THF) at 25 °C. Non-polarized images: (a) and (c). Crossed-Nicols images: (b) and (d).

Results and Discussion

Structural Characteristics of Bulk and Concentrated Solutions. Figure 2 illustrates q dependence of the scattering intensity I for bulk ATODC and cATODC samples at 180 °C; note that substantially the same result was obtained at 160 °C. Only a broad peak is found at q = 2.08 nm^{-1} for all the samples with a slight shoulder around 4 nm^{-1}. No appreciable signal was found in the lower q range down to q = 0.03 nm^{-1} as shown in Supporting Information. It should be noted that upward trend at the highest q is from the Kapton (polyimide) film set in the beamline. The peak position corresponds to the d-spacing of 3.02 nm. This value is consistent with the chain diameter of 3.2 nm estimated by the SAXS profile in dilute solution.[13] A similar broad peak was also found for concentrated MHK and THF solutions of ATODC and cATODC at somewhat lower q range. The actual q value at the peak slightly depends on the sample and concentration, that is, q = 1.6 – 1.7 nm^{-1} for ATODC in MHK (0.31 < c / g mL^{-1} < 0.40), q = 1.6 – 1.8 nm^{-1} for ATODC in THF (0.25 < c / g mL^{-1} < 0.40), q = 1.6 – 1.8 nm^{-1} for cATODC in MHK (0.45 < c / g mL^{-1} <

0.70), and q = 1.7 – 2.1 nm^{-1} for cATODC in THF (0.45 < c / g mL^{-1} < 0.50); note that the concentration were not very accurate because it was hard to prepare uniform solution in the capillary cell. This range q = 1.6 – 2.1 nm^{-1} is converted to the d-spacing of 3.0 – 4.0 nm which is similar or slightly larger than that for bulk at high temperature. Furthermore, no appreciable peak was found at low-q region (q > 0.03 nm^{-1}). These results indicate that no significant structure such as smectic superstructure exist in the current system and furthermore local alignment of the polymer chains are not very different between linear and cyclic chains.

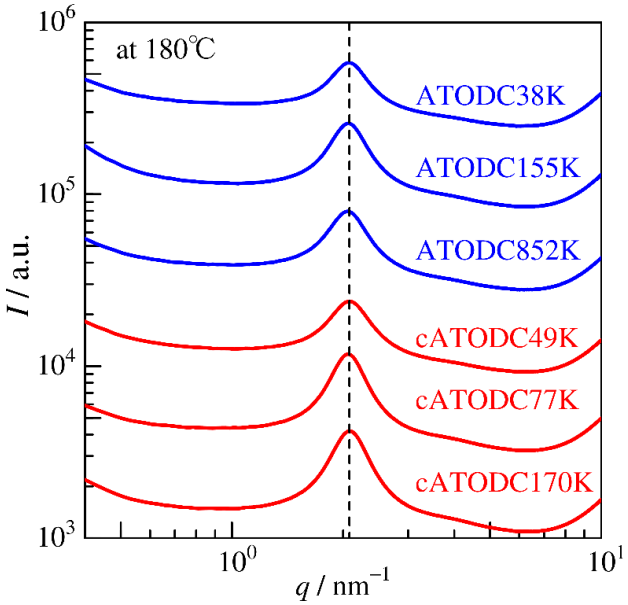

Figure 2. Plots of scattering intensity I versus the magnitude q of the scattering vector for the indicated samples at 180 °C. A dashed line, q = 2.08 nm^{-1}.

Phase Diagram of Lyotropic Systems. Results from phase separation experiments for ATODC and cATODC in the two solvents are summarized in Figure 3, in which c_0 values are plotted against the volume fraction Φ_{LC} of liquid crystal phase. Two phase boundary concentrations c_I and c_A were estimated as extrapolated values to Φ_{LC} = 0 and 1, respectively. The obtained data are plotted against the weight-average molar mass M_w in Figure 4. The phase boundary concentrations for linear ATODC samples are the slight decreasing function of M_w. This is a typical feature of semiflexible linear polymers in solution.[2] The data for ATODC in THF are appreciably smaller than those for the other amylose alkylcarbamate derivatives with shorter alkyl side chain. The phase boundary for the cyclic chains are quite higher than the linear chains, which is similar tendency with that for star branched chains[5, 6] while the M_w dependence seems to be more fluctuating.

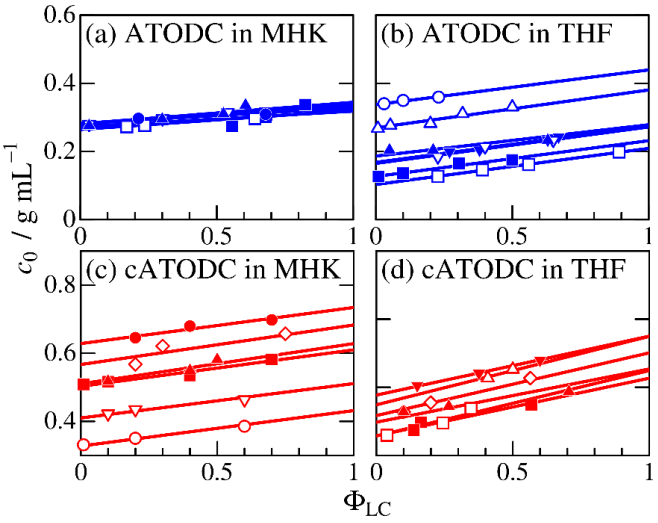

Figure 3. Plots of c_0 versus Φ_{LC} for ATODC in MHK (a), ATODC in THF (b), cATODC in MHK (c), and cATODC in THF (d) all at 25 °C. For panels (a) and (b), **ATODC25K** (unfilled circles), **ATODC38K** (filled circles), **ATODC102K** (unfilled triangles), **ATODC155K** (filled triangles), **ATODC164K** (unfilled inverted triangles), **ATODC284K** (filled inverted triangles), **ATODC852K** (unfilled squares), **ATODC1510K** (filled squares). For panels (c) and (d), **cATODC45K** (unfilled circles), **cATODC49K** (filled circles), **cATODC58K** (unfilled triangles), **cATODC77K** (filled triangles), **cATODC89K** (unfilled inverted triangles), **cATODC96K** (filled inverted triangles), **cATODC122K** (unfilled squares), **cATODC170K** (filled squares), **cATODC191K** (unfilled diamonds).

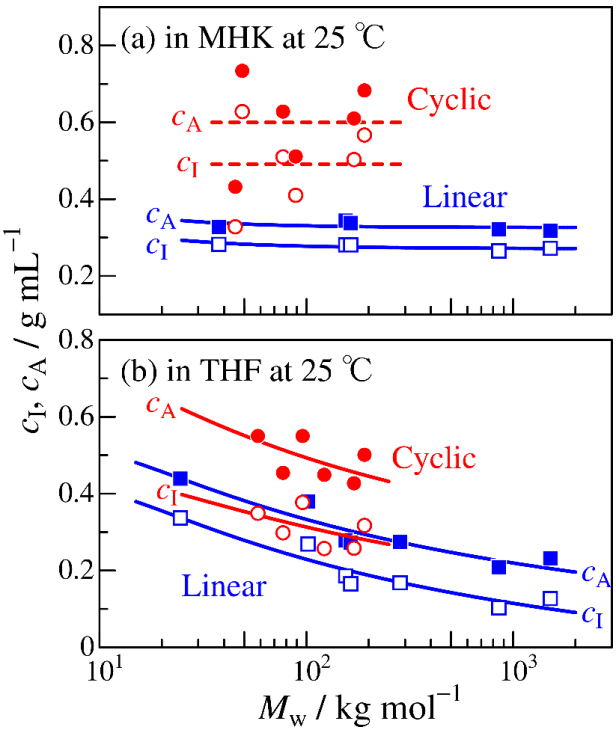

Figure 4. M_w dependence of c_I (unfilled symbols) and c_A (filled symbols) for ATODC (blue squares) and cATODC (red circles) in MHK (a) and in THF (b) at 25 °C.

Analysis of the Phase Diagram of Linear ATODC-Solvent Systems. We thus analyzed the phase diagram for linear ATODC in the two solvents in terms of the scaled particle theory (SPT) for the wormlike spherocylinder model,[2, 21, 22] which is characterized by the three parameters, the contour length L, the cylinder diameter d, and the Kuhn segment number N_K which is related to the Kuhn segment length λ^{-1} as $N_K = \lambda L$. According to Sato and Teramoto,[2] the mixing Helmholtz energy ΔA of the solution including n hard spherocylinders with L, d, and N_K is expressed as

$$\Delta A/n = \mu^{\circ} + k_B T F_L\left(c', L, d, N_K, \alpha\right) \tag{1}$$

where $\mu°$, k_B, T, c', and α are the standard chemical potential, the Boltzmann constant, the absolute temperature, the number concentration, and the degree of orientation, respectively; note that the terms of N_k disappears in the isotropic phase. This theory is applicable not only for rigid synthetic polymers but also polysaccharide derivatives.[12, 23, 24] The helix pitch h per residue defined by $h = LM_0/M_w$ was used instead of L to calculate c_I and c_A as a function of M_w. Assuming h and λ^{-1} from dilute solution properties,[13] that is, h = 0.36 nm and λ^{-1} = 45 nm in MHK and h = 0.40 nm and λ^{-1} = 24 nm in THF, d and α are needed to calculate ΔA at fixed μ_0, c', and T. The theoretical value can be evaluated as a solution of the following simultaneous equations with the osmotic pressure Π and the chemical potential μ of the spherocylinder

$$\Pi_{iso}\left(c_I\right) = \Pi_{nem}\left(c_A\right), \quad \mu_{iso}\left(c_I\right) = \mu_{nem}\left(c_A\right), \quad \partial A/\partial\alpha = 0 \tag{2}$$

where the subscripts iso and nem indicate the quantities of the isotropic and nematic phases, respectively. When we choose d = 2.8 nm and 3.8 nm for ATODC-MHK and ATODC-THF systems, respectively, the resultant theoretical values fairly explain the experimental phase boundaries as shown in Figure 5. These d values are quite larger than the thermodynamic chain diameter d_v = 2.2 – 2.3 nm which is defined as

$$d_v = \sqrt{\frac{4M_0\bar{v}}{\pi N_A h}} \tag{3}$$

while d and d_v are close to each other for many other polymers[22] including amylose alkylcarbamates with shorter side chains.[12] This is most likely because brush-like side alkyl chains swell in the solvent. Indeed, similar discrepancy was also found for brush-like polystyrene in dichloromethane.[25, 26] The experimental biphasic region is somewhat wider than the theoretical value. One of the possible reasons is a quite wide molar mass distribution of the current ATODC samples. In any case, we conclude that phase boundaries of linear ATODC in the two solvents are successfully explained by means of SPT and previously evaluated chain conformation in dilute solution, and the lower phase boundaries than the amylose carbamates with shorter side chain is mainly due to the thicker main chain.

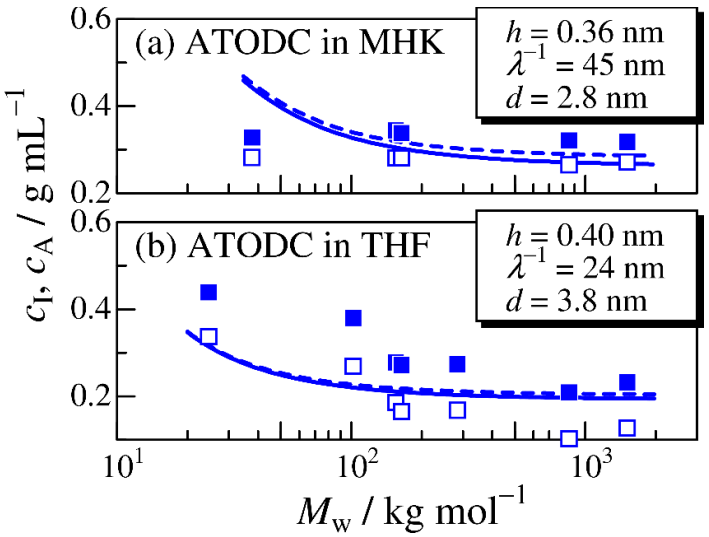

Figure 5. Comparison between experimental c_I (unfilled squares) and c_A (filled squares) for ATODC in MHK (a) and in THF (b) at 25 °C and the theoretical values for c_I (solid curve) and c_A (dashed curve) with the parameters listed in each panel.

Comparison with Theories: Cyclic ATODC-Solvent Systems. Since no applicable theory to describe thermodynamics of semiflexible ring in concentrated solution, we compared the phase diagram of cATODC in the two solvents with the Onsager theory for disk[27] with the diameter d_d and the length l_d. According to the theory, the two phase boundary concentrations c_I and c_A can be written as

$$c_I = 5.41 M N_A^{-1} d_d^{-3} \left[1 + 3.9 \left(l_d / d_d \right) + 1.27 \left(l_d / d_d \right)^2 \right]^{-1} \quad (4)$$

$$c_A = 1.34 c_I \quad (5)$$

where N_A and M are the Avogadro number and the molar mass of the solute, respectively. In order to apply this theory to the current ring polymer system, we assumed $l_d = d$ and $d_d = L/\pi + d$ as illustrated in Figure 6. When we calculate L from the dilute solution properties and assume that d is the same as that for the linear ATODC in the corresponding solvent, the resultant theoretical values plotted in Figure 7 are substantially smaller than the experimental data. Furthermore, the molar mass dependence is much more significant than the actual ring polymer. This might be because some part of actual ring polymers may exist inside the other ring chains, or conformation of the cATODC chain in the liquid crystalline phase is different from a rigid ring. According to the recent simulation and theoretical studies,[7, 8] rigid nanorings tend to form smectic phase in which columnar superstructure was found consisting of cumulated rings. On the contrary, SAXS data shown in the previous section indicate no significant diffraction reflecting such superstructures. Furthermore, a broad peak for cATODC at high q range was substantially the same as that for the corresponding linear chain. These results predict that cATODC chains in the liquid crystal phase form an extended conformation as shown in Figure 6c. This rodlike conformation may be possible because cycloamylose has rodlike conformation with antiparallel two helices in the crystalline state.[28-30] Furthermore, superhelical cyclic DNA is rodlike[4, 31] and cyclic DNA forms rodlike particle in polyplex micelles.[32, 33] If the cyclic polymer chains form rodlike structure in the liquid crystal phase, the phase boundary concentrations can be calculated by a simple expansion of SPT for the linear chain as in the case of our recent study for a rigid star polymer.[6]

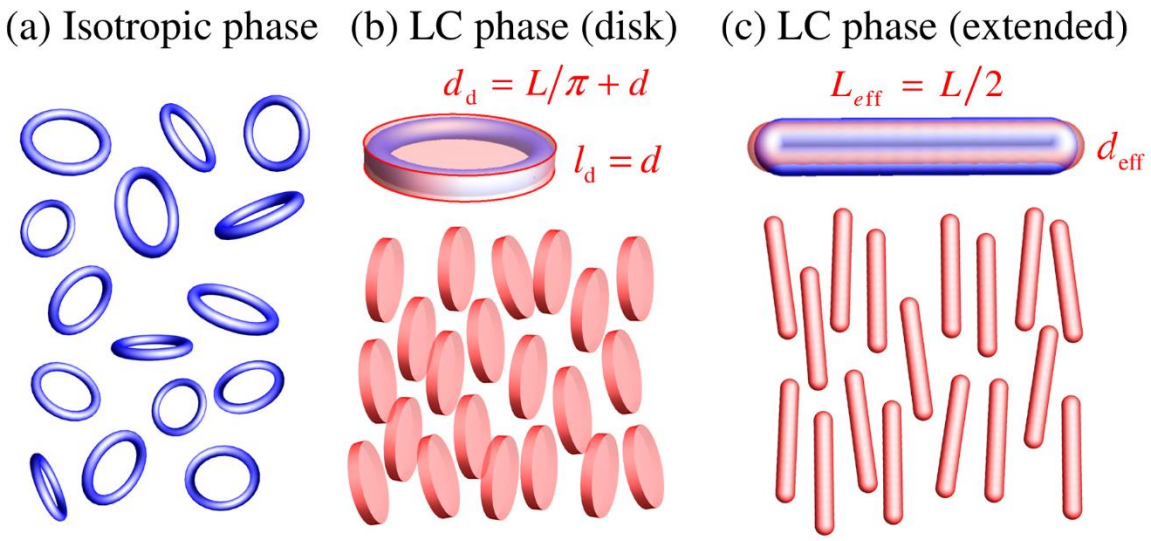

Figure 6. Schematic representation of the chain conformation of cATODC chains in the isotropic phase (a), in liquid crystal phase with disk-like conformation (b) and with rodlike conformation (c).

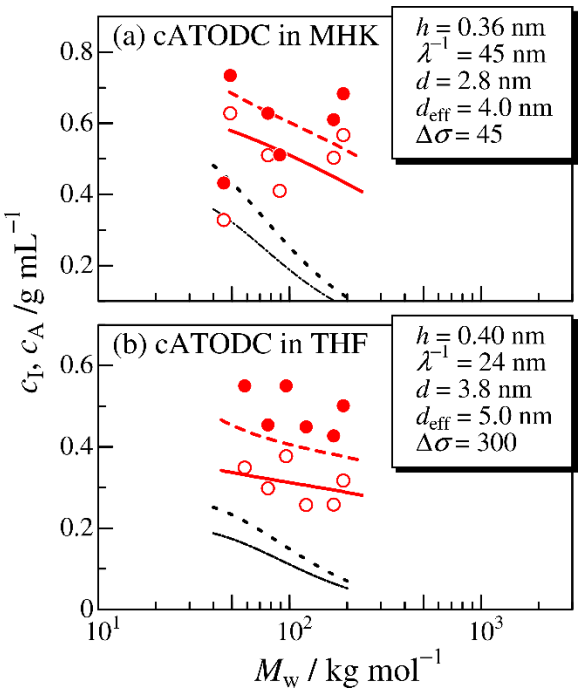

Figure 7. Comparison between experimental c_I (unfilled squares) and c_A (filled squares) for cATODC in MHK (a) and in THF (b) at 25 °C and the theoretical values for c_I (red solid curve) and c_A (red dashed curve) calculate in terms of the modified SPT. Black dot curve and dot dashed curve indicate the theoretical values for the Onsager theory for the disk (see text).

We thus analyzed the phase diagram in terms of the modified SPT. Eq 1 is also applicable to calculate ΔA for cATODC in isotropic solution. When we assume the ring polymer forms the extended conformation in liquid crystal phase as shown in Figure 6c with the effective contour

length L_{eff} and the effective chain diameter d_{eff}, ΔA for liquid crystal cATODC solution can be calculated with the following F_{C} instead of F_{L}

$$F_{\mathrm{C}} = F_{\mathrm{L}}\left(c', L_{\mathrm{eff}}, d_{\mathrm{eff}}, N_{\mathrm{K}}, \alpha\right) + \Delta\sigma \quad \text{(liquid crystal phase)} \qquad (6)$$

Here, $\Delta\sigma$ is the additional orientation and conformational entropy to confine the cyclic chain in the rodlike space. Assuming the wormlike chain parameters, h, λ^{-1}, and d are the same as that for ATODC in the corresponding solvent and $L_{\mathrm{eff}} = L/2$, the remaining parameters are d_{eff} and $\Delta\sigma$. If we choose d_{eff} = 4.0 nm and $\Delta\sigma$ = 45 for the cATODC-MHK system and d_{eff} = 5.0 nm and $\Delta\sigma$ = 300 for the cATODC-THF system, the theoretical phase boundary concentration in Figure 7 fairly explain the experimental phase diagram. The obtained d_{eff} value is possible because it is ca. 1.3 times larger than d. The additional entropy term $\Delta\sigma$ is larger than that for star polymer, that is, $\Delta\sigma$ = 20 or 32 depending on the assumed conformation in the liquid crystal, possibly suggesting that more compensation was needed to confine the cATODC chain in the extended rodlike conformation comparing with the star polymer. It should be however noticed that slight difference in λ^{-1} between linear and cyclic chains depicted in our previous papers,[11, 13, 34, 35] as well as topological repulsive interactions[36, 37] may be included in the parameter $\Delta\sigma$. The current SAXS data as well as the analysis of the phase diagram of cATODC in the two solvent systems suggested that the extended rodlike conformation in the liquid crystal phase is preferable while it behaves as wormlike ring in dilute solution. To confirm this specific conformational property, some other method is desirable to determine the conformation in the concentrated anisotropic solution.

Conclusions

Isotropic-liquid crystal phase diagrams of linear and cyclic ATODC were determined in the two solvent systems, MHK and THF. Structural characteristics both for linear and cyclic chains determined by means of SAXS over a wide q range have substantially the same each other. The phase boundary concentrations for linear ATODC in MHK and THF were successfully explained by the scaled particle theory (SPT) for the wormlike spherocylinder. While the phase diagram for cATODC samples cannot be explained by a disk model, it can be reproduced by a modified SPT originally developed for a star polymer assuming the cyclic polymer chains form rodlike conformation in the nematic phase.

Supporting Information

Additional SAXS data. This material is available free of charge via the Internet at http://pubs.acs.org.

Acknowledgments

The authors are grateful to Prof. Takahiro Sato (Osaka University) for fruitful discussion and to Dr. Noboru Ohta (SPring-8) for SAXS measurements. The synchrotron radiation experiments were performed at the BL40B2 in SPring-8 with the approval of the Japan Synchrotron Radiation Research Institute (JASRI) (proposal nos. 2016B1088, 2017A1082 and 2017B1062). This work was partly supported by JSPS KAKENHI grant numbers JP17K05884 and JP18H02020.

References

1. Tschierske, C. Development of structural complexity by liquid-crystal self-assembly. *Angew. Chem. Int. Ed.* **2013,** 52 (34), 8828-78 DOI: 10.1002/anie.201300872.

2. Sato, T.; Teramoto, A. Concentrated solutions of liquid-crystalline polymers. *Adv. Polym. Sci.* **1996,** 126, 85-161 DOI: 10.1007/3-540-60484-7_3.
3. Shibaev, V., 1.10 - Liquid Crystalline Polymers. In *Polymer Science: A Comprehensive Reference*, Matyjaszewski, K., Möller, M., Eds. Elsevier: Amsterdam, 2012; pp 259-285.
4. Zakharova, S. S.; Jesse, W.; Backendorf, C.; van der Maarel, J. R. Liquid crystal formation in supercoiled DNA solutions. *Biophys. J.* **2002,** 83 (2), 1119-29 DOI: 10.1016/S0006-3495(02)75235-1.
5. Goodson, S. H.; Novak, B. M. Synthesis and Characterization of Wormlike Three-arm Poly(*n*-hexyl isocyanate) Star Polymers. *Macromolecules* **2001,** 34 (12), 3849-3855 DOI: 10.1021/ma991692i.
6. Hasegawa, H.; Terao, K.; Sato, T.; Nagata, Y.; Suginome, M. Lyotropic Liquid Crystallinity of Linear and Star Poly(quinoxaline-2,3-diyl)s: Isotropic-Liquid Crystal Phase Equilibria in Tetrahydrofuran. *Macromolecules* **2019,** 52 (9), 3158-3164 DOI: 10.1021/acs.macromol.9b00460.
7. Avendano, C.; Jackson, G.; Muller, E. A.; Escobedo, F. A. Assembly of porous smectic structures formed from interlocking high-symmetry planar nanorings. *Proc. Natl. Acad. Sci. U. S. A.* **2016,** 113 (35), 9699-703 DOI: 10.1073/pnas.1604717113.
8. Wensink, H. H.; Avendano, C. Empty smectic liquid crystals of hard nanorings: Insights from a second-virial theory. *Physical review. E* **2016,** 94 (6-1), 062704 DOI: 10.1103/PhysRevE.94.062704.
9. Avendano, C.; Jackson, G.; Wensink, H. H. Nanorings in planar confinement: the role of repulsive surfaces on the formation of lacuna smectics. *Mol. Phys.* **2018,** 116 (21-22), 2901-2910 DOI: 10.1080/00268976.2018.1484950.
10. Terao, K.; Shigeuchi, K.; Oyamada, K.; Kitamura, S.; Sato, T. Solution Properties of a Cyclic Chain Having Tunable Chain Stiffness: Cyclic Amylose Tris(*n*-butylcarbamate) in Θ and Good Solvents. *Macromolecules* **2013,** 46 (13), 5355-5362 DOI: 10.1021/ma400774r.
11. Ryoki, A.; Ida, D.; Terao, K. Scattering function of semi-rigid cyclic polymers analyzed in terms of worm-like rings: cyclic amylose tris(phenylcarbamate) and cyclic amylose tris(n-butylcarbamate). *Polym. J.* **2017,** 49 (8), 633-637 DOI: 10.1038/pj.2017.27.
12. Oyamada, K.; Terao, K.; Suwa, M.; Kitamura, S.; Sato, T. Lyotropic Liquid Crystallinity of Armylose Tris(alkylcarbamates): Cholesteric and Smectic Phase Formation in Different Solvents. *Macromolecules* **2013,** 46 (11), 4589-4595 DOI: Doi 10.1021/Ma400787c.
13. Ryoki, A.; Kim, D.; Kitamura, S.; Terao, K. Linear and cyclic amylose derivatives having brush like side groups in solution: Amylose tris(n -octadecylcarbamate)s. *Polymer* **2018,** 137, 13-21 DOI: 10.1016/j.polymer.2017.12.063.
14. Gray, D. G. Chiral Nematic Ordering of Polysaccharides. *Carbohydr. Polym.* **1994,** 25 (4), 277-284 DOI: Doi 10.1016/0144-8617(94)90053-1.
15. Nishio, Y.; Sato, J.; Sugimura, K., Liquid Crystals of Cellulosics: Fascinating Ordered Structures for the Design of Functional Material Systems. In *Cellulose Chemistry and Properties: Fibers, Nanocelluloses and Advanced Materials*, Rojas, O. J., Ed. Springer International Publishing: Cham, 2016; pp 241-286.
16. Ishii, H.; Sugimura, K.; Nishio, Y. Thermotropic liquid crystalline properties of (hydroxypropyl)cellulose derivatives with butyryl and heptafluorobutyryl substituents. *Cellulose* **2019,** 26 (1), 399-412 DOI: 10.1007/s10570-018-2176-6.

17. Kitamura, S.; Yunokawa, H.; Mitsuie, S.; Kuge, T. Study on Polysaccharide by the Fluorescence Method .2. Micro-Brownian Motion and Conformational Change of Amylose in Aqueous-Solution. *Polym. J.* **1982,** 14 (2), 93-99 DOI: 10.1295/Polymj.14.93.
18. Waldmann, H.; Gygax, D.; Bednarski, M. D.; Randall Shangraw, W.; Whitesides, G. M. The enzymic utilization of sucrose in the synthesis of amylose and derivatives of amylose, using phosphorylases. *Carbohydr. Res.* **1986,** 157 (0), c4-c7 DOI: 10.1016/0008-6215(86)85078-9.
19. Takaha, T.; Yanase, M.; Takata, H.; Okada, S.; Smith, S. M. Potato D-Enzyme Catalyzes the Cyclization of Amylose to Produce Cycloamylose, a Novel Cyclic Glucan. *J. Biol. Chem.* **1996,** 271 (6), 2902-2908.
20. Nakata, Y.; Amitani, K.; Norisuye, T.; Kitamura, S. Translational Diffusion Coefficient of Cycloamylose in Aqueous Sodium Hydroxide. *Biopolymers* **2003,** 69 (4), 508-516 DOI: 10.1002/bip.10393.
21. Sato, T.; Teramoto, A. Statistical-Mechanical Theory for Liquid-Crystalline Polymer-Solutions. *Acta Polym.* **1994,** 45 (6), 399-412 DOI: DOI 10.1002/actp.1994.010450601.
22. Sato, T.; Shoda, T.; Teramoto, A. Scaled Particle Theory for Wormlike Hard Spherocylinders - Calculation of Phase-Diagrams for Ternary-Systems Consisting of 2 Semiflexible Polymers with Different Lengths and a Solvent. *Macromolecules* **1994,** 27 (1), 164-170 DOI: Doi 10.1021/Ma00079a024.
23. Sato, T.; Shimizu, T.; Kasabo, F.; Teramoto, A. Isotropic−Cholesteric Phase Equilibrium in Solutions of Cellulose Tris(phenyl carbamate). *Macromolecules* **2003,** 36 (8), 2939-2943 DOI: 10.1021/ma021786j.
24. Kuse, Y.; Asahina, D.; Nishio, Y. Molecular Structure and Liquid-Crystalline Characteristics of Chitosan Phenylcarbamate. *Biomacromolecules* **2009,** 10 (1), 166-173 DOI: 10.1021/bm801073e.
25. Maeno, K.; Nakamura, Y.; Terao, K.; Sato, T.; Norisuye, T. Liquid crystallinity of concentrated solutions of polymacromonomers consisting of polystyrene. *Kobunshi Ronbunshu* **1999,** 56 (4), 254-259.
26. Nakamura, Y.; Koori, M.; Li, Y.; Norisuye, T. Lyotropic liquid crystal formation of polystyrene polymacromonomers in dichloromethane. *Polymer* **2008,** 49 (22), 4877-4881 DOI: DOI 10.1016/j.polymer.2008.08.049.
27. Onsager, L. The Effects of Shape on the Interaction of Colloidal Particles. *Ann. N.Y. Acad. Sci.* **1949,** 51 (4), 627-659 DOI: DOI 10.1111/j.1749-6632.1949.tb27296.x.
28. Gessler, K.; Uson, I.; Takaha, T.; Krauss, N.; Smith, S. M.; Okada, S.; Sheldrick, G. M.; Saenger, W. V-Amylose at atomic resolution: X-ray structure of a cycloamylose with 26 glucose residues (cyclomaltohexaicosaose). *Proc. Natl. Acad. Sci. U. S. A.* **1999,** 96 (8), 4246-51 DOI: 10.1073/pnas.96.8.4246.
29. Nimz, O.; Gessler, K.; Uson, I.; Sheldrick, G. M.; Saenger, W. Inclusion complexes of V-amylose with undecanoic acid and dodecanol at atomic resolution: X-ray structures with cycloamylose containing 26 D-glucoses (cyclohexaicosaose) as host. *Carbohydr. Res.* **2004,** 339 (8), 1427-37 DOI: 10.1016/j.carres.2004.02.030.
30. Schnupf, U.; Momany, F. A. DFT energy optimization of a large carbohydrate: cyclomaltohexaicosaose (CA-26). *J Phys Chem B* **2012,** 116 (23), 6618-27 DOI: 10.1021/jp208927v.
31. Bates, A. D.; Maxwell, A., *DNA topology*. Oxford University Press, USA: 2005.
32. Männistö, M.; Vanderkerken, S.; Toncheva, V.; Elomaa, M.; Ruponen, M.; Schacht, E.; Urtti, A. Structure–activity relationships of poly(l-lysines): effects of pegylation and molecular

shape on physicochemical and biological properties in gene delivery. *J. Controlled Release* **2002,** 83 (1), 169-182 DOI: 10.1016/s0168-3659(02)00178-5.
33. Osada, K. Versatile DNA folding structures organized by cationic block copolymers. *Polym. J.* **2019,** 51 (4), 381-387 DOI: 10.1038/s41428-018-0157-0.
34. Asano, N.; Kitamura, S.; Terao, K. Local Conformation and Intermolecular Interaction of Rigid Ring Polymers Are Not Always the Same as the Linear Analogue: Cyclic Amylose Tris(phenylcarbamate) in Theta Solvents. *J. Phys. Chem. B* **2013,** 117 (32), 9576-83 DOI: 10.1021/jp406607w.
35. Ryoki, A.; Yokobatake, H.; Hasegawa, H.; Takenaka, A.; Ida, D.; Kitamura, S.; Terao, K. Topology-Dependent Chain Stiffness and Local Helical Structure of Cyclic Amylose Tris(3,5-dimethylphenylcarbamate) in Solution. *Macromolecules* **2017,** 50 (10), 4000-4006 DOI: 10.1021/acs.macromol.7b00706.
36. des Cloizeaux, J. Ring Polymers in Solution - Topological Effects. *J. Phys. Lett.* **1981,** 42 (19), L433-L436.
37. Ida, D.; Nakatomi, D.; Yoshizaki, T. A Monte Carlo Study of the Second Virial Coefficient of Semiflexible Ring Polymers. *Polym. J.* **2010,** 42 (9), 735-744 DOI: 10.1038/pj.2010.61.

Supporting Information for

Lyotropic Liquid Crystallinity of Linear and Cyclic Amylose Derivatives: Amylose Tris(*n*-octadecylcarbamate) in Tetrahydrofuran and 2-Octanone

DongChan Kim,[†] Akiyuki Ryoki,[†,‡] Daigo Kabata,[†] Shinichi Kitamura,[§] and Ken Terao*[,†]

[†]Department of Macromolecular Science, Graduate School of Science, Osaka University, 1-1 Machikaneyama-cho, Toyonaka, Osaka, 560-0043, Japan

[‡]Department of Polymer Chemistry, Graduate School of Engineering, Kyoto University, Katsura, Kyoto 615-8510, Japan

[§]Center for Research and Development of Bioresources, Organization for Research Promotion, Osaka Prefecture University, 1-2, Gakuen-cho, Naka-ku, Sakai, 599-8570, Japan

E-mail: kterao@chem.sci.osaka-u.ac.jp

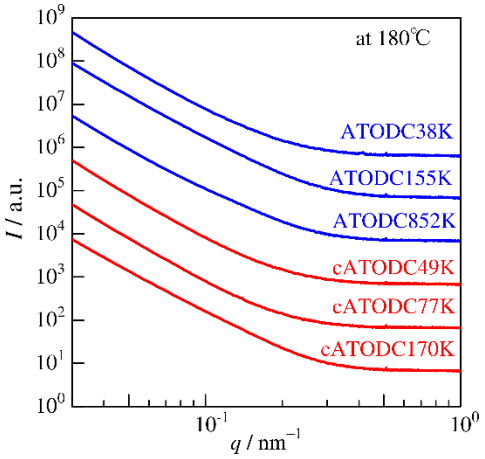

Figure S1. Plots of scattering intensity I versus the magnitude q of the scattering vector for the indicated samples at 180 °C in the USAXS q range.

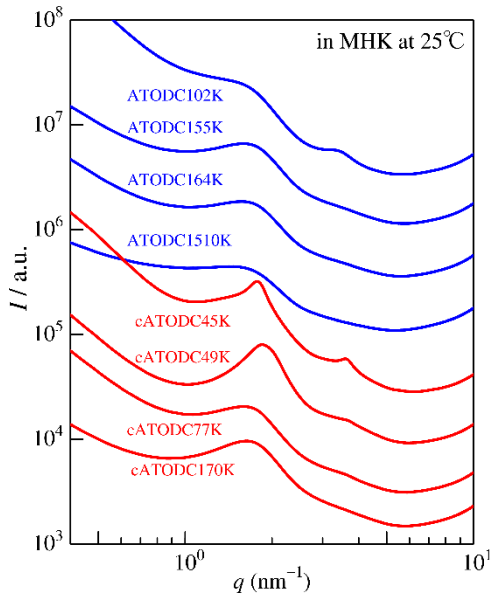

Figure S2. Plots of scattering intensity I versus q for **ATODC102K** (c = 0.4 g mL^{-1}), **ATODC155K** (c = 0.35 g mL^{-1}), **ATODC164K** (c = 0.35 g mL^{-1}), **ATODC1510K** (c = 0.35 g mL^{-1}), **cATODC45K** (c = 0.45 g mL^{-1}), **cATODC49K** (c = 0.7 g mL^{-1}), **cATODC77K** (c = 0.6 g mL^{-1}), **cATODC170K** (c = 0.6 g mL^{-1}) all in MHK at 25 °C.

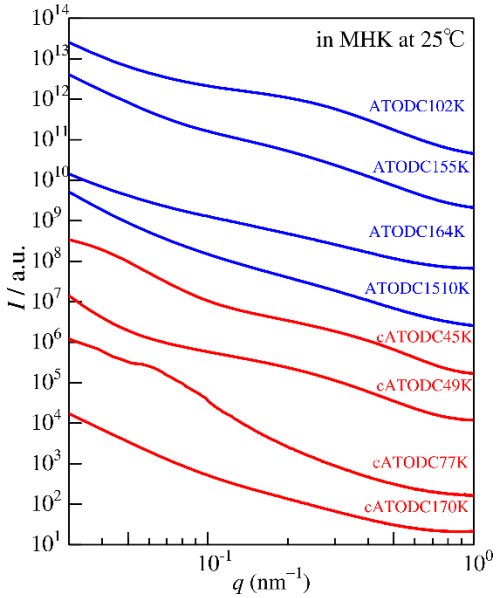

Figure S3. Plots of scattering intensity I versus q for indicated ATODC and cATODC samples in MHK at 25 °C (USAXS range).

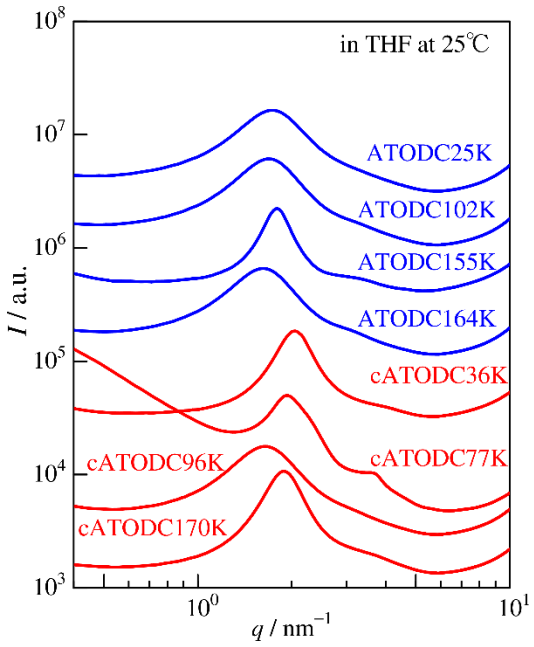

Figure S4. Plots of scattering intensity I versus q for **ATODC25K** (c = 0.4 g mL^{-1}), **ATODC102K** (c = 0.35 g mL^{-1}), **ATODC155K** (c = 0.25 g mL^{-1}), **ATODC164K** (c = 0.28 g mL^{-1}), **cATODC36K** (c = 0.45 g mL^{-1}), **cATODC77K** (c = 0.5 g mL^{-1}), **cATODC96K** (c = 0.45 g mL^{-1}), **cATODC170K** (c = 0.45 g mL^{-1}) all in THF at 25 °C.

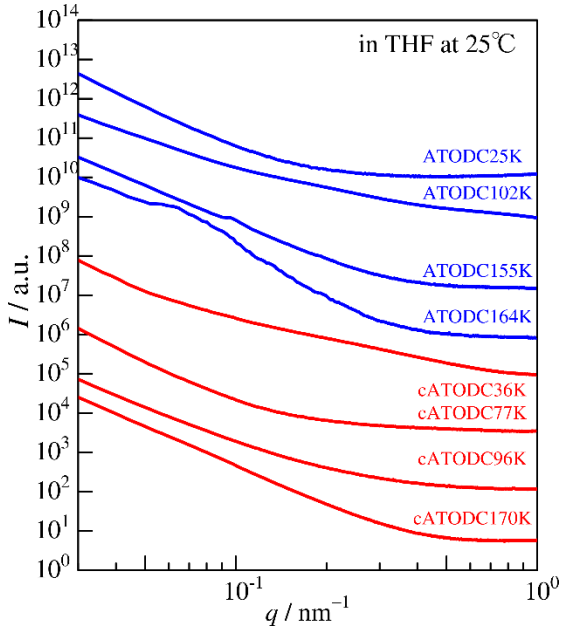

Figure S5. Plots of scattering intensity I versus q for indicated ATODC and cATODC samples in THF at 25 °C (USAXS range).